Thermally-insulated ultra-fast high temperature sintering (UHS) of zirconia: a master sintering curve analysis

Jian Dong[a], Vaclav Pouchly[b], Mattia Biesuz[c,d], Václav Tyrpekl[d], Monika Vilémová[c], Milad Kermani[a], Mike Reece[e], Chunfeng Hu[a] , Salvatore Grasso[a,*]

[a] Key Laboratory of Advanced Technologies of Materials, Ministry of Education, School of Materials Science and Engineering, Southwest Jiaotong University, Chengdu 610031, China
[b] Brno University of Technology, 62100 Brno, Czech Republic
[c] Institute of plasma physics of the Czech Academy of Sciences, Za Slovankou 3, 182 00 Prague, Czech Republic
[d] Department of Inorganic Chemistry, Faculty of Science, Charles University, Hlavova 8, 2030 Prague, Czech Republic
[e] Queen Mary, University of London, Mile End Road, London, E1 4NS, UK

* Corresponding author:
Prof. Salvatore Grasso, s.grasso@swjtu.edu.cn
School of Materials Science and Engineering
Southwest Jiaotong University
Chengdu 610031, China

Abstract

A thermally-insulated Ultra-fast High temperature Sintering (UHS) has been developed to maximize the densification of 3 mol% yttria-stabilized zirconia and improve the energy efficiency of the process. Thermally-Insulated UHS (TI-UHS) employed a fibreboard insulator, which reduced the energy consumption by ≈40% compared to the reference set-up. An ultrafast heating rate, approaching ≈2000 °C/min, produced dense (99% relative density) and fine-grained (178±18 nm) microstructures within 60 s. By cross-linking finite element simulations with master sintering curves a good fit between experimental and predicted density was obtained, allowing the development of predictive models for UHS densification.

Keywords: 3YSZ, Grain Size, Ultra-fast sintering, Master sintering curve

Because of their unique combination of mechanical, thermal, biological, and electrochemical properties, zirconia ceramics suit a wide range of applications: as dental materials [1,2], thermal barrier coatings [3], solid-oxide fuel cells [4,5], oxygen sensors [6] and cutting tools. Pure zirconia results in three different polymorphs, which are stable at different temperatures: monoclinic (T < 1170°C), tetragonal (1170 < T < 2400°C), and cubic (T > 2700°C). The tetragonal phase is mainly employed in structural components since it possesses high mechanical strength and excellent fracture toughness (~ 10 MPa $m^{1/2}$) due to the well-known phase transformation toughening effect. On the other hand, cubic ZrO_2 possesses excellent ionic conductivity and is therefore employed in electrochemical devices. Cubic and tetragonal polymorphs are stabilized by doping with bivalent and trivalent oxides like Y_2O_3, Sc_2O_3, Yb_2O_3, CaO and MgO.

In the past few years, there has been a renewed interest in ultrafast sintering techniques [7] to reduce the processing time as well as the energy consumed during the firing cycle of ceramics. Besides the clear environmental and energetic advantages of fast sintering schedules, they are also thought to enhance densification and limit grain growth [8–12] as discussed for flash, fast firing, microwave and, spark plasma sintering. In other words, it has been suggested that grain growth and densification kinetics can be decoupled and exploited to produce dense and fine-grained materials.

Recently, Wang et.al. developed Ultra-fast High-temperature Sintering (UHS) [13]. In UHS, a green body is introduced within a graphite felt, which is quickly Joule heated. The process allows extremely rapid heating (≈10^3-10^4 °C/min [14]) up to high temperatures (≈3000°C) that can be controlled in real-time by programming the electric power dissipation on the graphite felt heater. The rapid heating schedule is thought to facilitate densification while suppressing the low-temperature activated grain coarsening mechanisms, similar to what has been reported for flash sintering [8,11,12]. Furthermore, it is suggested that the apparent activation energy for densification could decrease due to fast heating [13]. However, any densification pathway prediction suffers from the intrinsic uncertainty about the real heating schedule of the sample. This makes it difficult to build predictive models able to estimate the sample density evolution and to understand whether or not densification is accelerated by the extreme heating conditions.

Another limitation of UHS is that most of the heat produced in the felts is radiated toward the surrounding and is not concentrated in the sample. This limits the energy efficiency of the process. A similar problem is also encountered in flash sintering and can be limited using suitable thermal insulators [15,16].

In this work, we have developed predictive models able to estimate the density evolution upon UHS. The ability to predict final density based on the thermal history was verified by combining finite element method (FEM) simulations and master sintering curves (MSC). This made it possible to investigate whether or not UHS densification is enhanced by fast heating. For this purpose, 3YSZ was chosen as a model system. Moreover, we proposed a Thermally-Insulated UHS process (hereinafter TI-UHS) to limit radiative heat loss experienced in the original setup.

The 3YSZ powder was premixed with a binder (commercial TZ-3YSB-E, Tosoh, 90 nm crystallite size). The raw powder was weighed (0.5 g) and then shaped in a steel die using a uniaxial press (hydraulic press YLJ-40T, MTI corporation, China) at 100 MPa. The sample diameter was 13 mm and its thickness ≈1.2 mm. Finally, the disk-shaped samples were debinded and pre-sintered at 1000 °C for 60 min (after this step the relative density was as low as 48 ± 3.5%) at a heating rate of 10 °C/min in a conventional furnace (XD-1700M, Zhengzhou Brother Furnace Co., Ltd., China). After that, the pre-sintered samples were placed between two pieces of carbon felt (80×30×5 mm^3, SGL carbon Co., Germany), and two different experimental setups were employed (**Figure 1**):

(i) UHS (original set up): the carbon felts were not thermally insulated.
(ii) Thermally-insulated UHS (TI-UHS): Al_2O_3 fibreboard insulator (80×30×30 mm^3, W-FMF1700) was placed around the graphite felt;

The felts were then connected to a power supply (0-30V, 0-100A, SOYI-30100DM, Shanghai Soyi Power Co., Ltd., China). The power supply was computer-controlled (holding time, current, voltage). The applied electric current was 25-40 A (≈ 80-130 kA/m^2) and was maintained for different times of up to 60 s. The experiments were carried out within an argon-filled glove box (flowing 10-15 l/min) to avoid oxidation of carbon felt (see Fig.S1).

Finally, the density of the samples (a set of 3 for each conditions) was measured using the Archimedes' method, and their fracture cross-section was observed using a SEM (GeminiSEM, ZEISS 300). Before that, the samples were polished and thermal etched at 1200°C at a heating rate of 10 °C/min for 60 min.

The temperature distribution of 3YSZ was quantified using a COMSOL simulation model developed in Ref. [17]. The model was validated against the melting point of Platinum and Palladium wires as discussed in Fig.S2. The reproducibly of calibration experiments gave an error of within ±5% of the set electrical current (corresponding to ±1.75 A in the case of 35 A) and such error propagated to the simulated temperatures. The electrical current and voltage were measured using a two channels data logger (DPT3010, Guangdong Shenzheng Juwei Co., Ltd.). Temperatures up to 1450 °C were recorded using a K-type thermocouple in contact with the sample.

The density obtained upon UHS was compared with those predicted using the master sintering curve model (MSC) for 3YSZ. The MSC was determined using dilatometric data recorded at different heating rates (2, 5, 10 and 20 °C/min) by a high-temperature dilatometer (L75, Linseis, Germany). The dilatometric tests were carried out on 3YSZ samples prepared similarly to the UHS ones and cut into prism shapes of about 10 mm length. Starting from the densification profiles [18], a MSC was determined by the specialized software "Density MSC" with the use of Mean Perpendicular Curve Distance as the criterion for finding the optimal activation energy of sintering Q [19]. The prediction of densification profiles for different heating rates (10, 100, 1000, 1700, 10000 °C/min) was done by calculating the MSC time-temperature integral using the Density MSC software as described in Ref. [19].

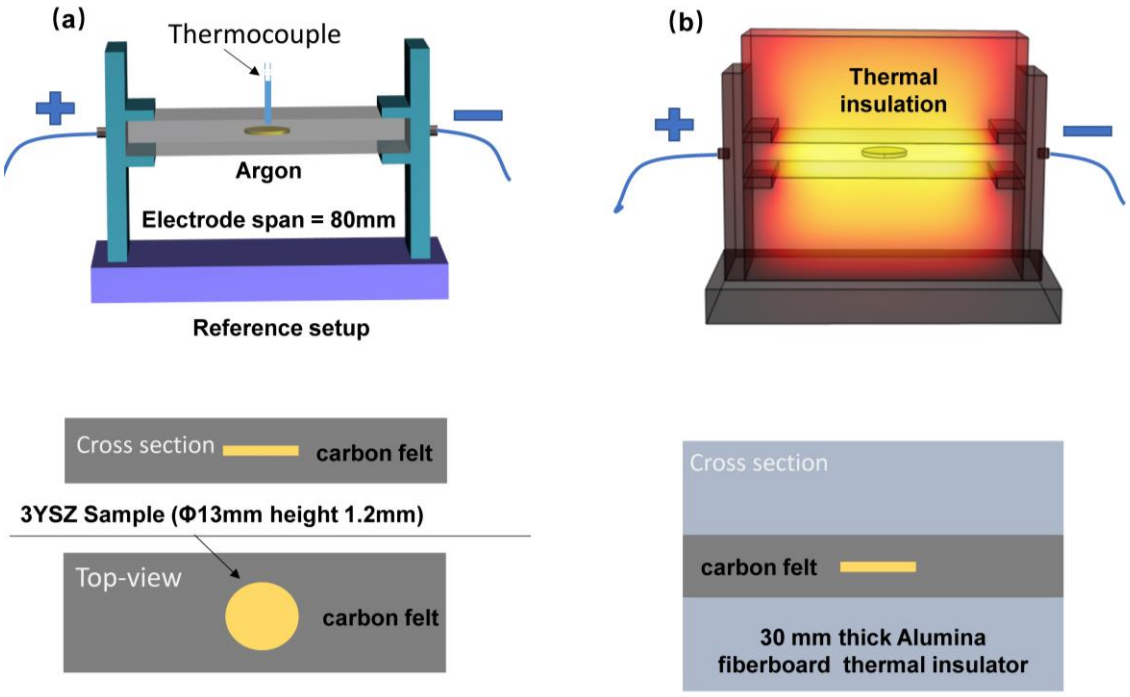

Figure 1. The schematic of (a) reference UHS setup according to Wang et al. [13]; and (b) thermally insulated (TI-UHS) proposed in this work.

Figure 2 compares the temperature evolution determined by FEM simulations at the center mid-thickness of the specimens UHSed (35 A, 60 s) with and without thermal insulation. The estimated thermal gradients within the 1.2 mm thick specimen were within 20 °C, thus we can consider that the sample temperature was effectively homogeneous during the process.

The FEM simulations were compared with the temperature profiles recorded using a K-thermocouple contacting the sample in the case of UHS without thermal insulation (**Figure 2(a)**). On the other hand, because of the very high temperature (max >1800 °C) experienced in TI-UHS we could not identify a suitable thermocouple (i.e. commercially available thermocouples were unsuitable because either electrically unshielded or too thick) and so temperatures were estimated by calibrated simulations using the melting point of Pt as reference (**Figure S1**). The modelled and experimental temperature evolution are in good agreement, thus pointing out that the FEM model provides an acceptable approximation of the thermal history of the sample.

Note that the peak temperature was substantially different using the original UHS and thermally-insulated UHS setup (though the same electric parameters were used). In fact, the maximum temperature reached without thermal insulation was about 1420-1450°C, whereas temperatures exceeding 1750°C were estimated for TI-UHS. In the first part of the TI-UHS heating cycle (until ≈1000°C), the temperature increases almost linearly with time (**Figure 2(d)**) and with the consumed electric energy (**Figure 2(f)**), with the heating rate approaching 3000°C/min. Furthermore, the differences between UHS and TI-UHS are rather limited below 1000°C. This suggests that most of the electric energy is used to heat the UHS system (felts and sample) and the heat losses are not particularly relevant.

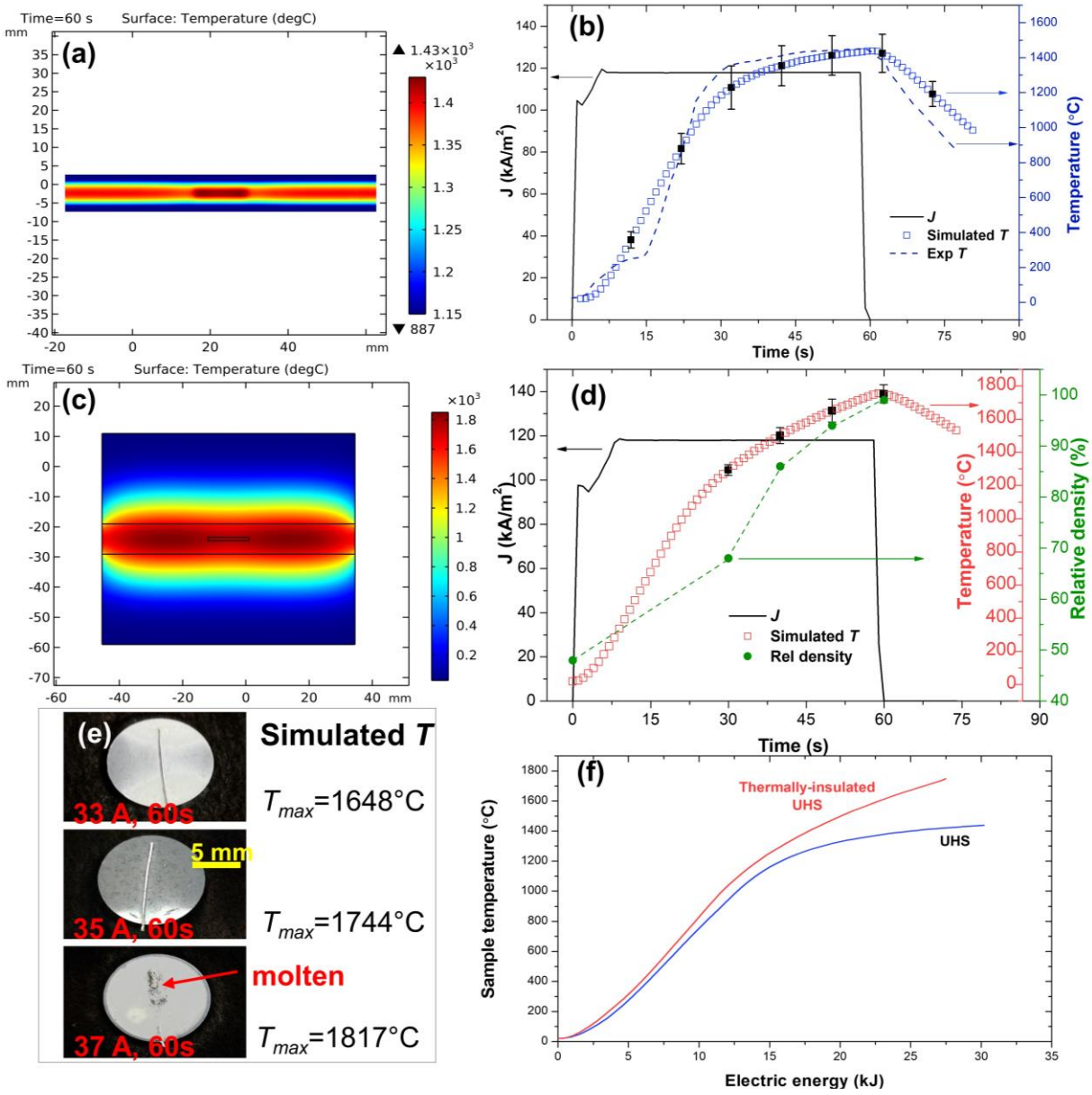

Figure 2. Simulated temperature distribution for (a,b) UHS and (c,d) thermally-insulated UHS. FEM predicted temperature is represented by blue squares and error bar of Temperature in black squares, the dashed line in (b) reports the temperature measured with a K-thermocouple. (e) FEM calibration experiments for TI-UHS, the platinum wire melts between 35 and 37 A in agreement with the simulated temperature (melting point Pt = 1768°C). (f) sample temperature evolution as a function of the input electric energy for TI-UHS and non-insulated UHS.

However, as the felts temperature increases, the heat losses become more and more relevant, in particular by radiation. For this reason, the heating rate progressively decreases and temperature tends to stabilize in the case of non-insulated UHS. In other words, the system approaches a condition where the heat produced by the Joule effect is matched by the radiation losses. On the contrary, the use of the alumina insulator significantly reduces the heat losses in TI-UHS, and the temperature continues to substantially grow (though at a lower rate). Therefore, TI-UHS appears to be a very promising set-up for improving the efficiency of UHS, especially when temperatures exceeding 1000°C are required. In the case of the reference UHS setup, the energy consumed to reach 1424°C within 60 s, calculated using measured voltage

and current, was 30 kJ. When an alumina fibreboard was employed, the same temperature was reached within 36 s with a significant drop in consumed energy down to 18 kJ.

The different thermal cycles experienced by the sample with and without thermal insulation impacted the microstructure of the UHSed bodies (**Table 1** and **Figure 3**). In fact, the bulk density of samples treated under 35 A for 60 s was 68 ± 3.2% and 99 ± 0.5% for samples UHSed without and with thermal insulation, respectively. These results are confirmed by the SEM micrographs in **Figure 3**: a very porous microstructure was retained when the samples were UHSed without thermal insulation, whereas a full-dense and fine-grained (178 ± 18 nm) material was achieved in the case of TI-UHS. In particular, TI-UHS produced microstructures which resemble those typically achieved in 3YSZ by other fast sintering techniques like flash sintering (120-150 nm [11,20]) and fast firing (≈ 210 nm [21]), where it is usually assumed that densification dominates over grain coarsening because of rapid heating. In previous works, it has been also reported that fast heating in UHS could significantly lower the apparent activation energy for densification [13]. To follow the temporal evolution of density during TI-UHS (35 A), experiments were interrupted at different stages 30, 45, and 50 s. The final relative density and the peak temperature for different TI-UHSed samples are listed in **Table 1**. Obviously, the final density increases when increasing the processing time from 30 s (55%) to 60 s (99%) under 35 A.

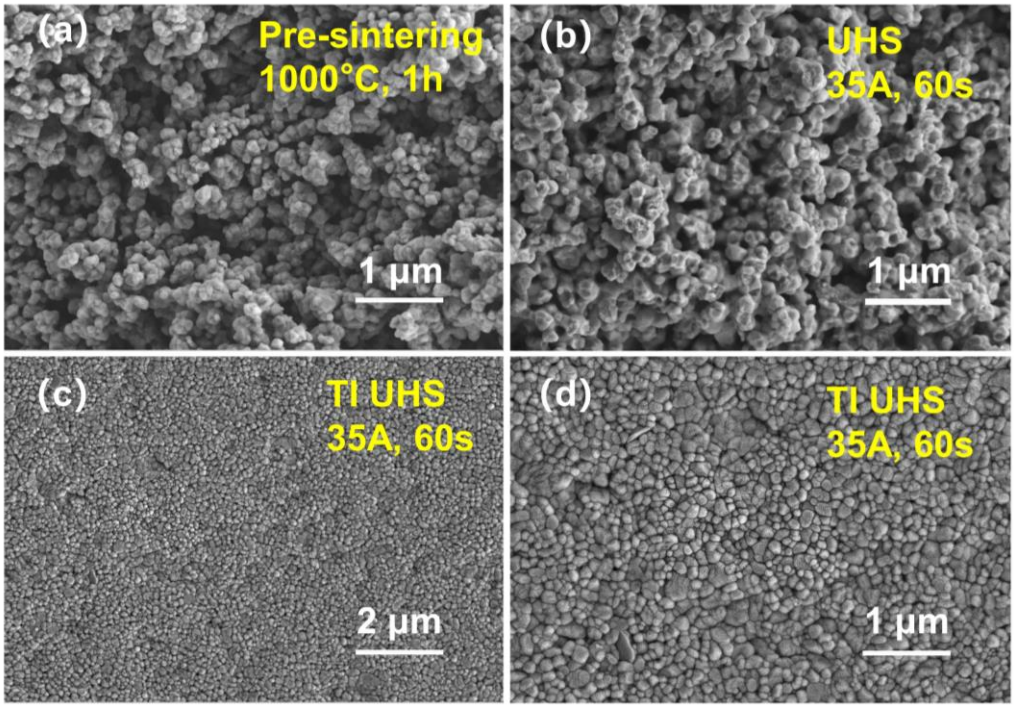

Figure 3. SEM micrographs of fracture section of (a) starting green body heated pre-sintered at1000°C; (b) UHS treatment without insulator under 35A for 60 s; (c,d) thermally insulated UHS 35A for 60 s at low and high magnification.

To investigate the UHS densification mechanisms, we compared the density evolution in the TI-UHS samples (35 A- 30, 45, 50, 60 s) with that expected from the master sintering curves calculated on the same material. The samples prepared under the same conditions but without thermal insulation were porous and therefore not of interest. The MSC approach was originally developed by Su and Johnson [22] to calculate the density of a component starting from their

thermal history. Integrating the differential equations for combined-stage sintering models [23] one can get [24]:

$$\frac{k}{\gamma\Omega D_0}\int_{\rho_0}^{\rho}\frac{(G(\rho))^n}{3\rho\Gamma(\rho)}d\rho=\int_0^t\frac{1}{T}\exp\left(-\frac{Q}{RT}\right)dt$$

with

$$\Theta(t,T(t))\equiv\int_0^t\frac{1}{T}\exp\left(-\frac{Q}{RT}\right)dt$$

where γ is the surface energy, Ω is the atomic volume, k is the Boltzmann constant, T is the absolute temperature, G is the mean grain size, t is the time, D_0 is the pre-exponential constant of the self-diffusion coefficient, and Γ represents geometric factors. The term Θ represents the work of sintering and is a function of thermal history. If the microstructure (i.e., the grain size) is a function of density only (i.e., it is independent on the densification pathway), then a bijective function correlates Θ and ρ. In other words, it is possible to calculate ρ knowing the thermal history, Θ.

Fig. 4(a) shows MSC constructed from the dilatometric analysis carried out at 2, 5, 10, and 20 °C/min using Q as a fitting parameter. The inset shows that the mean residual squares have a minimum at $Q \approx 680$ kJ/mol, which is a slightly larger but not far different from literature values (typically between 500 and 600 kJ/mol [25,26] for finer grade than the one employed in the present study). The overlap between individual heating rates is not ideal, however, it is mostly caused by the slight difference between the green densities of the individual green bodies. Based on the calculated Q, it is, possible to build a prediction map (**Figure 4(b)**) for various heating rates (2 – 10000 °C/min). As can be seen in the 3D map, with the increasing heating rate, densification is slightly shifted to higher temperature values.

Table 1. The TI-UHS experimentally measured and predicted relative density using master sintering curves for different discharge times using a current of 35 A and thermally insulated setup.

Sample code	Processing time (s)	Simulated temperature (°C)	Relative density (%)	Predicted density from MSC (%)
Pre-sintered	0	-	48	-
UHS 1	30	1268±32	55±3.0	58.0±0.9
UHS 2	45	1604±48	87±2.5	90.9±0.6
UHS 3	50	1710±69	94±2.0	98.4±0.2
UHS 4	60	1755±55	99±0.5	99.4±0.3

The expected final density of the UHSed samples was calculated using the MSC and the thermal history estimated from the FEM simulations (**Table 1**). The predicted density of 58, 90.9, 98.4, 99.4% (see **Fig.S3(b)**) showed a good fit with the experimental data, to within a deviation of 3.5%. This allows us to draw some useful conclusions:

i. The MSC approach combined with FEM simulations allows the predictive models to be built that are able to determine the density evolution upon UHS;
ii. The densification of 3YSZ upon UHS follows the MSC, thus the previously claimed significant heating rate effect on the apparent activation energy for sintering [27] appears unlikely, at least in the case of 3YSZ;

iii. The hypothesis behind the MSC model remains substantially valid during UHS; in other words, we have found no direct evidence to support the idea that fast heating produces additional mechanisms that promote densification upon UHS of ceramics, using 3YSZ as a model material. This observation contradicts previous finding on flash sintered YSZ, where the application of an electric field seems to reduce the sintering activation energy. Further studies are needed to provide a more comprehensive comparison between the different fast firing techniques.

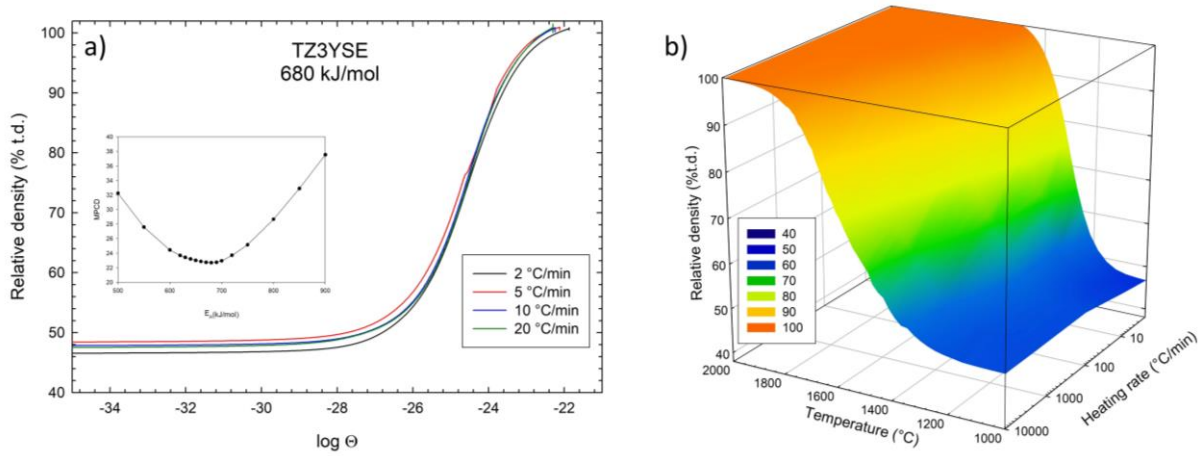

Figure 4. a) Master Sintering Curve constructed for TZ3YSE powder, with insert of criterion used to estimate the activation energy of sintering of 680 kJ/mol. b) Predicted densification map using master sintering curve approach assuming no dwelling time and neglecting shrinkage upon cooling.

In summary, 99% dense 3YSZ samples can be produced within 60 s by Thermally-Insulated UHS under 35 A, whereas the standard UHS setup (without insulator) led to poor densification (RD: 68%). This indicates that the heat loss are extremely relevant in UHS and that the energy efficiency of the process can be greatly improved by TI-UHS. Meanwhile, dense TI-UHS sample possess a fine grained-microstructure (178±18 nm) similar to that typically achieved by other fast sintering methods (e.g. FS, FF). Finally, the predicted density evolution upon TI-UHS, estimated by combining Master Sintering Curve (MCS) and FEM methods, fit well with experimental results, providing a valuable tool for studying the densification process during UHS. The results seem to refute the idea that the fast heating boosts densification upon UHS of 3YSZ.

Acknowledgments
This work was supported by Thousand Talents Program of China and Sichuan Province (Grant number 5187020096) as well as by research grant of Brno University of Technology: FSI-S-20-6292. C H received support from the Natural Sciences Foundation of China (No.

52072311) Outstanding Young Scientific and Technical Talents in Sichuan Province (2019JDJQ0009).

References:

[1] L. Li, C. Zhao, Z. Du, Y. Qiu, W. Si, Int. J. Appl. Ceram. Technol. 16 (2019) 1830–1835.

[2] C.A. Maziero Volpato, L.G.D. Altoe Garbelotto, M. Celso, F. Bondioli, Adv. Ceram. - Electr. Magn. Ceram. Bioceram. Ceram. Environ. (2011).

[3] F. Zhang, D. Sun, J. Xie, S. Xu, H. Huang, J. Li, H. Hou, J. Wu, Int. J. Heat Technol. 35 (2017) 765–772.

[4] A. Hammou, Solid Oxide Fuel Cells, 2008.

[5] A. Atkinson, S.J. Skinner, J.A. Kilner, Encycl. Sustain. Sci. Technol. (2012).

[6] L. Shuaishuai, Z. Jiaqiao, N. Hongjun, H. Haiqin, W. Xingxing, T. Jianbing, K. Wenxiu, J. Phys. Conf. Ser. 1345 (2019).

[7] M. Biesuz, S. Grasso, V.M. Sglavo, Curr. Opin. Solid State Mater. Sci. 24 (2020).

[8] W. Ji, B. Parker, S. Falco, J.Y. Zhang, Z.Y. Fu, R.I. Todd, J. Eur. Ceram. Soc. 37 (2017) 2547–2551.

[9] M.O. Prado, M. Biesuz, M. Frasnelli, F.E. Benedetto, V.M. Sglavo, J. Non. Cryst. Solids 476 (2017) 60–66.

[10] V. Esposito, E. Traversa, J. Am. Ceram. Soc. 91 (2008) 1037–1051.

[11] W. Ji, J. Zhang, W. Wang, Z. Fu, R. Todd, J. Eur. Ceram. Soc. 40 (2020) 5829–5836.

[12] Y. Zhang, J. Nie, J.M. Chan, J. Luo, Acta Mater. 125 (2017) 465–475.

[13] C. Wang, W. Ping, Q. Bai, H. Cui, R. Hensleigh, R. Wang, A.H. Brozena, Z. Xu, J. Dai, Y. Pei, C. Zheng, G. Pastel, J. Gao, X. Wang, H. Wang, J.C. Zhao, B. Yang, X. Zheng, J. Luo, Y. Mo, B. Dunn, L. Hu, Science (80-.). 368 (2020) 521–526.

[14] R.F. Guo, H.R. Mao, Z.T. Zhao, P. Shen, Scr. Mater. 193 (2021) 103–107.

[15] M. Biesuz, J. Dong, S. Fu, Y. Liu, H. Zhang, D. Zhu, C. Hu, S. Grasso, Scr. Mater. 162 (2019) 99–102.

[16] J. Liu, X. Li, X. Wang, R. Huang, Z. Jia, Scr. Mater. 176 (2020) 28–31.

[17] S. Grasso, Y. Sakka, N. Rendtorff, C. Hu, G. Maizza, H. Borodianska, O. Vasylkiv, J. Ceram. Soc. Japan 119 (2011) 144–146.

[18] K. Maca, V. Pouchly, A.R. Boccaccini, Sci. Sinter. 40 (2008) 117–122.

[19] V. Pouchly, K. Maca, Sci. Sinter. 42 (2010) 25–32.

[20] M. Cologna, B. Rashkova, R. Raj, J. Am. Ceram. Soc. 93 (2010) 3556–3559.

[21] S.Y. Gómez, A.L. Da Silva, D. Gouvêa, R.H.R. Castro, D. Hotza, Mater. Lett. 166 (2016) 196–200.

[22] H. Su, D.L. Johnson, J. Am. Ceram. Soc. 79 (1996) 3211–3217.

[23] J.D. Hansen, R.P. Rusin, M. -H Teng, D.L. Johnson, J. Am. Ceram. Soc. 75 (1992) 1129–1135.

[24] T. Frueh, I.O. Ozer, S.F. Poterala, H. Lee, E.R. Kupp, C. Compson, J. Atria, G.L. Messing, J. Eur. Ceram. Soc. 38 (2018) 1030–1037.

[25] R. Caruso, N. Mamana, E. Benavidez, J. Alloys Compd. 495 (2010) 570–573.

[26] M. Mazaheri, A. Simchi, M. Dourandish, F. Golestani-Fard, Ceram. Int. 35 (2009) 547–554.

[27] W.Q. Shao, S.O. Chen, D. Li, H.S. Cao, Y.C. Zhang, S.S. Zhang, 31 (2008) 903–906.